Available online at www.sciencedirect.com

ScienceDirect

Advances in Space Research 59 (2017) 794–803

ADVANCES IN SPACE RESEARCH (a COSPAR publication)

www.elsevier.com/locate/asr

Rapid ambiguity resolution over medium-to-long baselines based on GPS/BDS multi-frequency observables

Xiaopeng Gong [a], Yidong Lou [a,c], Wanke Liu [b,c,*], Fu Zheng [a], Shengfeng Gu [a], Hua Wang [c,d]

[a] GNSS Research Center, Wuhan University, 129 Luoyu Road, Wuhan, Hubei 430079, China
[b] School of Geodesy and Geomatics, Wuhan University, 129 Luoyu Road, Wuhan, Hubei 430079, China
[c] Collaborative Innovation Centre for Geospatial Technology, 129 Luoyu Road, Wuhan, Hubei 430079, China
[d] Department of Surveying Engineering, Guangdong University of Technology, 100 Waihuan Xi Road, Guangzhou, China

Received 14 March 2016; received in revised form 29 June 2016; accepted 6 July 2016
Available online 16 July 2016

Abstract

Medium-long baseline RTK positioning generally needs a long initial time to find an accurate position due to non-negligible atmospheric delay residual. In order to shorten the initial or re-convergence time, a rapid phase ambiguity resolution method is employed based on GPS/BDS multi-frequency observables in this paper. This method is realized by two steps. First, double-differenced un-combined observables (i.e., L1/L2 and B1/B2/B3 observables) are used to obtain a float solution with atmospheric delay estimated as random walk parameter by using Kalman filter. This model enables an easy and consistent implementation for different systems and different frequency observables and can readily be extended to use more satellite navigation systems (e.g., Galileo, QZSS). Additional prior constraints for atmospheric information can be quickly added as well, because atmospheric delay is parameterized. Second, in order to fix ambiguity rapidly and reliably, ambiguities are divided into three types (extra-wide-lane (EWL), wide-lane (WL) and narrow-lane (NL)) according to their wavelengths and are to be fixed sequentially by using the LAMBDA method. Several baselines ranging from 61 km to 232 km collected by Trimble and Panda receivers are used to validate the method. The results illustrate that it only takes approximately 1, 2 and 6 epochs (30 s intervals) to fix EWL, WL and NL ambiguities, respectively. More epochs' observables are needed to fix WL and NL ambiguity around local time 14:00 than other time mainly due to more active ionosphere activity. As for the re-convergence time, the simulated results show that 90% of epochs can be fixed within 2 epochs by using prior atmospheric delay information obtained from previously 5 min. Finally, as for positioning accuracy, meter, decimeter and centimeter level positioning results are obtained according to different ambiguity resolution performances, i.e., EWL, WL and NL fixed solutions.

Keywords: GPS/BDS; Medium-long baseline; Rapid ambiguity resolution; Multi-frequency observables

1. Introduction

Currently, medium-long baseline (more than 20 km) RTK has a broad range of applications, such as providing location information in a sparse reference network or in marine areas. It is well-known that rapid and reliable ambiguity resolution (AR) is necessary for high-precision applications of global navigation satellite system (GNSS) positioning. For medium-long baseline RTK, AR is affected by non-negligible double differenced (DD) atmospheric delay residuals. A number of efforts have been made to improve the medium-long baseline RTK positioning by considering the DD atmospheric delay. The idea of weighting ionospheric delay, which is also regarded as pseudo-observables, can be found in the work of Bock et al. (1986), Teunissen (1997) and Odijk (2000). Among

* Corresponding author at: School of Geodesy and Geomatics, Wuhan University, 129 Luoyu Road, Wuhan, Hubei 430079, China.
E-mail address: wkliu@sgg.whu.edu.cn (W. Liu).

http://dx.doi.org/10.1016/j.asr.2016.07.011
0273-1177/

these, Odijk (2000) tested the method by using a permanent GPS network with a rather large inter-station spacing (100–200 km). The results illustrated that correct integers were instantaneously resolved with more than 80% of the epochs when the weighted corrections were applied. Concerning high-precision RTK applications, Yang et al. (2000) proposed an RTK algorithm by using an ionospheric information filter based on Kalman filter. The test results demonstrated that centimeter-level positioning could be achieved within 120 epochs (interval: 15 s) for baselines shorter than 50 km. However, the convergence time for ambiguity resolution increases with baseline length. Many approaches have been developed to enable high-accuracy GPS kinematic positioning by using a network of GPS reference stations (Cannon et al., 2001; Rizos, 2002; Hu et al., 2003; Paziewski, 2015). Since a network of GPS reference stations is not always available, Dekkiche et al. (2010) presented a model where the ionospheric delay parameter was treated as Gauss–Markov random process with a correlation time of 100 s for single-reference long baseline kinematic positioning. A 51 km baseline solution shows that the precision of horizontal coordinate and vertical component can be achieved in millimeter and 2 cm levels, respectively. Yanase et al. (2010) argued that more accurate positioning could be achieved with estimation of ionospheric and tropospheric gradients than without gradient estimation in both static and kinematic situations.

It has been anticipated that multi-constellation and multi-frequency observables will also benefit AR, though this may not help estimate atmospheric delay. In order to understand the potential of triple frequency observables on AR, three carrier ambiguity resolution (TCAR) and cascaded integer rounding (CIR) methods were proposed in the work of Forssell et al. (1997) and Jung (1999), respectively. Neglecting the DD ionospheric delay, both two methods could only provide an easy solution AR for short baselines. Furthermore, Teunissen et al. (2002) argued that TCAR and CIR methods were based on a geometry-free (GF) model and fixed ambiguity by using bootstrapping procedures, while the least-squares ambiguity decorrelation adjustment (LAMBDA Teunissen, 1995) method was based on a geometry-based (GB) model and fixed ambiguity by using an integer least-squares (ILS) method. Hence, the LAMBDA method would have a higher probability rate of success. From then on, more GB models were derived by extending the concepts and algorithms of TCAR or multiple carrier ambiguity resolution (MCAR) in the work of Vollath (2004), Feng and Rizos (2005) and Feng (2008). As for the contribution of multi-constellation, Verhagen (2002) argued that AR success rate of combined GPS and Galileo was better than each single system. Meanwhile, Tiberius et al. (2002) analyzed the performance of AR with GPS and Galileo observables and concluded that single epoch AR success rate would achieve a 95% level for 20–30 km baselines. As for long baseline computation, Chu and Yang (2014) concluded that the current level of accuracy of daily baseline solutions could be improved by using additional Galileo system. Moreover, he argued that single-system triple-frequency ambiguity resolution was more resistant to the influence of code noise and multipath errors than dual-frequency dual-constellation ambiguity resolution.

In the studies mentioned above, promising results have been obtained by using the additional constellation and third frequency signal. However, since no real tracking triple-frequency observables were available, those studies were conducted with simulated or semi-simulated signals. And due to the fact that BDS officially provides service in the Asia–Pacific region, many significant studies have been carried out to demonstrate the potential of triple-frequency observables and combined GPS/BDS in RTK positioning by using real tracking observables. Teunissen et al. (2014) demonstrated that ambiguity dilution of precision (ADOP) value would decrease and a high cut-off elevation could be used in RTK by combining GPS and BDS. Deng et al. (2014) analyzed the reliability of GPS/BDS dual-frequency AR and argued that multi-system observables could improve both AR reliability and position accuracy in short baseline RTK. The same results were also achieved in works of He et al. (2014), Odolinski et al. (2014), Tang et al. (2015) and Xu et al. (2015).

Though these studies show great improvement in RTK positioning when using network reference stations, multi-constellation or multi-frequency observables, the performance of medium-long baseline RTK still needs further analysis, especially for a single-reference station baseline. Therefore, we employ a rapid AR method for single-reference medium-long baseline RTK positioning based on GPS/BDS dual/triple frequency observables. Firstly, we give an introduction to the combined GPS/BDS RTK model based on Kalman filter. Secondly, the step-wise AR method is briefly introduced. Thirdly, several baselines ranging from 61 to 232 km are employed to test the method. The last part is the summary and conclusions.

2. Models and methods

In this section, we present the medium-long baseline RTK model combining GPS and BDS together with step-wise AR method. Since we focus on the DD mode, all expressions in the following sections, unless specified otherwise, denote DD.

2.1. Mathematic model

We apply system-specific DD and thus have one pivot satellite per system. For brevity, the DD operator $\Delta\nabla$ is omitted. DD GNSS observables on frequency f is defined as follows

$$\begin{aligned} P_f &= \rho + \alpha T_z + \beta_f I + \varepsilon_P \\ \Phi_f &= \rho + \alpha T_z - \beta_f I - \lambda_f N_f + \varepsilon_\Phi \end{aligned} \tag{1}$$

where P_f and Φ_f represent the DD pseudorange and carrier phase observables on frequency f ($f = 1, 2, 3$) in length units, respectively; ρ is the DD geometric distance, while antenna phase center corrections should be applied to P, Φ before ρ becomes unassociated with the frequency; T_z is the DD zenith tropospheric delay that can be converted to the slant delay with the mapping function α; β_f is the ionospheric scale factor (ISF); I denotes the DD slant ionospheric delay on P_1; N is the DD ambiguity, together with the corresponding wavelength λ; ε_P, ε_Φ represent observable noise of pseudorange and carrier phase, respectively. We use the model provided by Lou et al. (2016) to correct BDS code bias variations. Thus, the differential code bias (DCB) can be canceled by DD.

Assuming that n_G GPS satellites and n_B BDS satellites are tracked, the combined GPS/BDS RTK model can be defined as follows (Teunissen et al., 2014):

$$\mathrm{E}\begin{bmatrix} P \\ \Phi \end{bmatrix} = \begin{bmatrix} A & \Lambda & 0 \\ A & -\Lambda & C \end{bmatrix}\begin{bmatrix} a \\ b \\ c \end{bmatrix}, \quad \mathrm{D}\begin{bmatrix} P \\ \Phi \end{bmatrix} = \begin{bmatrix} Q_{PP} & 0 \\ 0 & Q_{\Phi\Phi} \end{bmatrix} \tag{2}$$

where E[.] and D[.] denote the expectation and dispersion operator, respectively; $P = [P_G, P_B]^T, \Phi = [\Phi_G, \Phi_B]^T$ represent DD code and carrier phase vector, respectively; a is baseline vector and tropospheric delay; $b = [I_G, I_B]$ denotes DD ionospheric delay; $c = [c_G, c_B]^T$ is the DD ambiguity vector; the other symbols are defined as follows:

$$\begin{aligned} A &= \begin{bmatrix} A_G & \alpha_G \\ A_B & \alpha_B \end{bmatrix}, \quad A_* = [e_{f_*} \otimes D_{s_*}^T F_*] \\ \Lambda &= \begin{bmatrix} \Lambda_G & 0 \\ 0 & \Lambda_B \end{bmatrix}, \quad \Lambda_* = \mathrm{diag}[\beta_{1_*}, \ldots \beta_{f_*}] \otimes U_{n_*} \\ C &= \begin{bmatrix} C_G & 0 \\ 0 & C_B \end{bmatrix}, C_* = \mathrm{diag}[\lambda_{1_*}, \ldots \lambda_{f_*}] \otimes U_{n_*} \end{aligned} \tag{3}$$

in which * is system flag with $^* = \{G,B\}(G = GPS, B = BDS)$; U_{n_*}}is the $n^* \times n^*$ unit matrix; e_{f_*} denotes $f^* \times 1$ vector of 1's; $D_{s_*}^T = [-e_{n_*}, I_{n_*}]$ is the $n^* \times (n^*+1)$ differencing matrix; F^* represents un-differenced receiver-satellite unit direction; $\otimes$ is the Kronecker product (Rao, 1973); and the entries of the positive definite variance matrix are given as:

$$\begin{aligned} Q_{PP} &= \begin{bmatrix} Q_{P_G P_G} & 0 \\ 0 & Q_{P_B P_B} \end{bmatrix}, Q_{\Phi\Phi} = \begin{bmatrix} Q_{\Phi_G \Phi_G} & 0 \\ 0 & Q_{\Phi_B \Phi_B} \end{bmatrix} \\ Q_{P_* P_*} &= C_{P_* P_*} \otimes 2Q_*, Q_{\Phi_* \Phi_*} = C_{\Phi_* \Phi_*} \otimes 2Q_* \\ C_{P_* P_*} &= \mathrm{diag}[\delta_{P_{1*}}^2, \cdots \delta_{P_{f*}}^2], C_{\Phi_* \Phi_*} = \mathrm{diag}[\delta_{\Phi_{1*}}^2, \ldots \delta_{\Phi_{f*}}^2] \\ Q_* &= D_{n_*}^T W_*^{-1} D_{n_*}, W_* = \mathrm{diag}[w_{1_*}, \ldots, w_{n_*+1}] \end{aligned} \tag{4}$$

where w_i^* is the satellite elevation dependent weight.

The above definitions allow for a compact representation of general GNSS models (Teunissen, 1997). If model (2) is applied in short baseline, the DD atmospheric parameter should be absent because they can be almost ignored. However, the DD tropospheric and ionospheric delay could not be ignored in the medium-long range baseline so they would be set as zero initially and estimated as a random walk in each processing session in this paper. As for stochastic model, it is better to use residual-based function than standard stochastic model (Jin et al., 2010), but it will cost more time. And the different stochastic model will only lead to millimeter to centimeter level difference in static positioning estimation (Jin et al., 2005). This is almost ignorable compared to the accuracy of float solution (meter level). Thus, the weight w_i^* is defined according to an elevation dependent-function given in Euler and Goad (1991) in our experiments. By solving Eq. (2), the baseline vector, atmospheric delay (for medium-long baseline) as well as float ambiguity vector can be determined by the Kalman filter.

2.2. Ambiguity resolution

By solving Eq. (2), we can obtain uncombined (i.e., DD L1/L2 or B1/B2/B3) float ambiguity vectors (c) and their variance–covariance matrix (Q_{cc}). It is known that triple frequency observables can form longer wavelength ambiguity than dual frequency observables, which will benefit the success rate and reliability of AR. Thus, a three-step AR method (EWL, WL and NL) is used to obtain a rapid and reliable AR. According to the work of Feng (2008), three combinations (EWL (0, −1, 1), WL (1, −1, 0) and NL (2, −1, 0)) are selected for medium-long baseline RTK. And the characteristics of these combinations are listed in Table 1. The symbol σ_{TN} represents the total noise level and σ_0 is the noise of phase observables. Moreover, the uncertainty term σ_{trop}, σ_{iono} and σ_{orb} represent the effects of respective bias or modeling/correction errors.

Based on the float solution, the LAMBDA method is applied to search for the optimal fixed value for each subset of ambiguities. In order to obtain a reliable ambiguity-fixed solution, the FF-ratio test (Verhagen and Teunissen, 2013) is applied to evaluate reliability. For each AR step, if they pass the FF-Ratio test (the fixed failure rate is set as 1%), these integer ambiguities will be applied as constrains to obtain the ambiguity-fixed solution (EWL fixed solution, WL fixed solution and NL fixed solution). Otherwise, the ambiguity resolution processing will break and start to process the next epoch.

The first step is to fix EWL ambiguity vectors. Because triple-frequency observables are only available for BDS, we only try to fix EWL (0, −1, 1) of BDS in this step. Based on the uncombined float ambiguities (c) and their variance–covariance matrix (Q_{cc}), the float EWL ambiguity vectors (N_{EWL}) and their variance–covariance matrix (Q_{EWL}) can be derived as follows:

$$N_{EWL} = T_{EWL} \cdot c_B, \quad Q_{EWL} = T_{EWL} \cdot Q_{c_B c_B} \cdot T_{EWL}^T \tag{5}$$

where $T_{EWL} = [\,0 \quad -1 \quad 1\,] \otimes U_{n_B}$ is the transition matrix. Once the EWL ambiguities are successfully fixed, we start the second step, to fix WL ambiguities. It should be noted

Table 1
Characteristics of the combinations for GPS and BDS.

System	Combination	Wavelength (m)	$\sigma_0 = 1$ (unit: cm)	
			$\sigma_{trop} = 2.5$ $\sigma_{iono} = 20$ $\sigma_{orb} = 5$	$\sigma_{trop} = 5$ $\sigma_{iono} = 40$ $\sigma_{orb} = 5$
			σ_{TN} (cycle)	
BDS	(0, −1, 1)	4.884	0.091	0.147
	(1, −1, 0)	0.847	0.288	0.545
	(2, −1, 0)	0.156	0.287	0.819
GPS	(1, −1, 0)	0.862	0.317	0.603
	(2, −1, 0)	0.156	0.279	0.781

that WL ambiguities of GPS and BDS are to be fixed in this step. The float WL ambiguity vectors (N_{WL}) and their variance–covariance matrix (Q_{WL}) are derived as follows:

$$N_{WL} = T_{WL} \cdot c, \quad Q_{WL} = T_{WL} \cdot Q_{cc} \cdot T_{WL}^{T} \tag{6}$$

where $T_{WL} = \text{blkdiag}[T_{WL_G}, T_{WL_B}]$ $(T_{WL_G} = [1 \quad -1] \otimes U_{n_G}$, $T_{WL_B} = [1 \quad -1 \quad 0] \otimes U_{n_B})$ is the transition matrix. If WL ambiguities are successfully fixed, the third step that tries to fix NL ambiguities is implemented. The float NL ambiguity vectors (N_{NL}) and variance–covariance matrix (Q_{NL}) of GPS and BDS are given as follows:

$$N_{NL} = T_{NL} \cdot c, Q_{NL} = T_{NL} \cdot Q_{cc} \cdot T_{NL}^{T} \tag{7}$$

where $T_{NL} = \text{blkdiag}[T_{NL_G}, T_{NL_B}]$ $(T_{NL_G} = [2 \quad -1] \otimes U_{n_G}$, $T_{NL_G} = [2 \quad -1 \quad 0] \otimes U_{n_B})$ is the transition matrix. Once NL ambiguities are successfully fixed, the three AR steps are all completed and we can obtain a NL-fixed solution. In each step, if AR passes FF-ratio test, additional constraints (constraining integer ambiguities) can be used to update parameters. To be more specific, the data processing strategy mentioned above is described in Fig. 1.

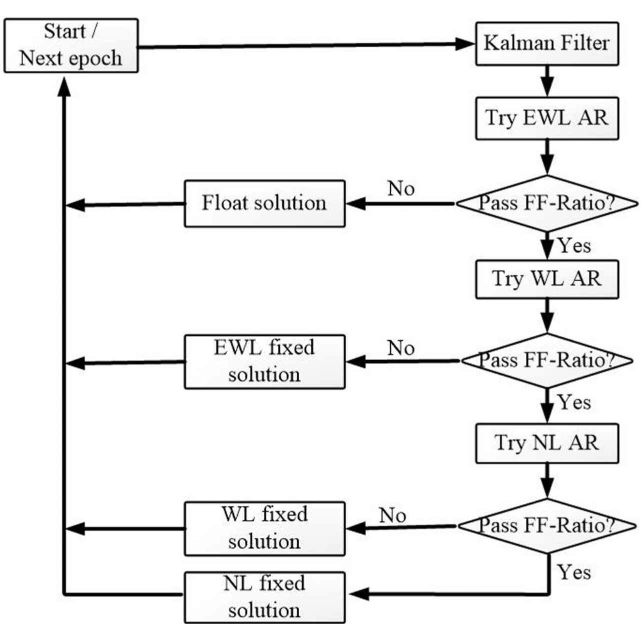

Fig. 1. Flowchart of processing.

3. Experiments and result analysis

In this section, several baselines, ranging from 61 km to 232 km, are employed to validate the proposed method for medium-long baseline RTK positioning.

3.1. Data collection and processing strategy

In the following experiment, 8 baselines ranging from 61 km to 232 km are tested. Table 2 gives the detailed information of each baseline. The test observables are collected by GPS/BDS dual/triple frequency receivers for 30 s sample intervals for all baselines. Unlike Trimble receiver, Panda receiver is manufactured by a Chinese company and its core OEM module is also made in China. In order to verify the method, the kinematic positioning mode is adopted to process static observables epoch by epoch, which means that the baseline vector of each epoch is not relevant. Nowadays, real-time precise orbit products of GPS have already been available due to the IGS real-time pilot project (RTPP). Besides, Wuhan University is able to provide real time multi-system precise orbit products in the near future. The accuracy of all these orbit products is quite close to post processing products. Thus, we adopt precise multi-system orbit products provided by GFZ since the accuracy of broadcast ephemeris is limited.

It is well-known that full AR is almost impossible at some time for medium-long baseline RTK, because observables with low elevation are generally involved with large multipath and atmospheric residuals. Fortunately, the number of visible satellites greatly increases when both GPS and BDS are used, which means a higher than customary cut-off angle can be used for RTK positioning (Teunissen et al., 2014). This is important for rapid AR in medium-long baseline RTK. Fig. 2 is an example of the DD ionospheric delay of baseline A and B. Fig. 2 shows that low elevation satellites generally have a larger ionospheric delay. For baseline A, the ionospheric delay around elevation 1° reaches approximately 3 meters around GPS time 11:00. Moreover, the ionospheric delay differs when changing baseline length, station location and observation time. Thus, it is very challenging to use a proper prior model to modeling this change and it is impossible to

Table 2
Baseline information.

Receiver type	No.	Doy, Year	Length (km)	Lat., Lon. (Degree)
Trimble Net R9	A	274–278, 2014	109	N32, E105
	B		144	N37, E112
	C		206	N31, E104
	D		232	N31, E100
Panda	E	317, 2015	61	N23, E116
	F		122	N23, E116
	G		147	N22, E116
	H		229	N21, E112

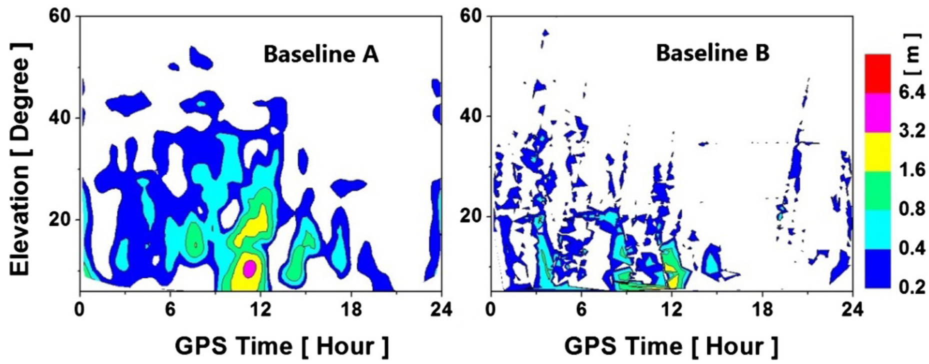

Fig. 2. Examples of DD ionospheric delay, DOY 274, 2014.

choose a priori fixed cut-off angle for different baselines. Since rapid AR is our focus, ionospheric delay may be not estimated well in a short time, especially for low elevation satellites. Hence, we use a partial AR method by setting the cut-off angle as 10° at first. According to the cut-off angle, a subset of ambiguities is chosen for AR. The cut-off angle is progressively increased by 5° until we fix ambiguity successfully or the number of ambiguities is less than 4.

3.2. Time-to-first-fix

Time-to-first-fix (TTFF) is the time to initially fix ambiguity, which reflects the initial time of RTK positioning. A small TTFF means we can easily reach a high-accuracy position within a short time. Since we only focus on TTFF in this section, the Kalman filter is reset as soon as ambiguities are fixed. For example, if we analyse TTFF of EWL ambiguity, ambiguities and atmospheric parameters are instantaneously reset when EWL ambiguities are fixed. Then, the average TTFFs of EWL, WL and NL can be calculated according to Eq. (8):

$$Average\ \ TTFF = \frac{\sum_{i=1}^{n} TTFF_i}{n} \tag{8}$$

where n is the number of fixed epochs.

Table 3 gives a summary of the TTFFs of EWL, WL and NL for all baselines. For comparison, the WL and NL TTFF of GPS-only are also given in Table 3. Compared to performance of GPS-only, the result shows a great improvement in TTFF when combining GPS and BDS together. For instance, it will take about 40 epochs to fix NL for GPS-only while it only need about 6 epochs for combined GPS and BDS. As for combined GPS and BDS, it is easily observed that EWL ambiguity can be fixed by every single epoch of all the baselines mainly due to the long wavelength of EWL ambiguity (approximately 4.8 m of BDS). Additionally, the average TTFF of WL ambiguity is only approximately 2 epochs, which is still fairly rapid., and there is only a minor difference in WL TTFF between different baselines. The best is approximately 1.3 epochs and the worst is approximately 3.0 epochs. It is not surprising that WL TTFF of baseline H is the worst because it has a long baseline length and locates in low latitudes. As for NL ambiguity, the average TTFF is approximately 6.0 epochs. Generally, the TTFF of NL increases with baseline length and station latitude. For example, baseline E, which is the shortest one, only takes 1.7 epochs to fix NL ambiguity. However, it needs 8.0 epochs to fix NL ambiuity for baseline H, which locates at the similar latitude with baseline E but has a longer baseline length. However, it seems that baseline C shows an abnormal performance of NL AR that it is even worse than baseline H.

Fig. 3 gives details of average TTFF of WL ambiguity for all baselines. It is obvious that more epochs are needed to fix WL ambiguity when ionospheric activity is high

Table 3
Statistical results of TTFFs.

Receiver Type	No. Average TTFFs (epochs) GPS/BDS GPS-only					
	EWL		NL	WL	WL	NL
Trimble NetR9	A	1.0	2.1	3.8	4.8	46.1
	B	1.0	1.7	3.7	3.7	28.3
	C	1.0	2.9	14.5	5.4	64.7
	D	1.0	2.2	5.4	4.3	50.5
Panda	E	1.0	1.3	1.7	2.9	45.0
	F	1.0	1.3	3.1	2.2	27.5
	G	1.0	1.5	4.7	2.6	29.4
	H	1.0	3.0	8.0	5.1	48.0

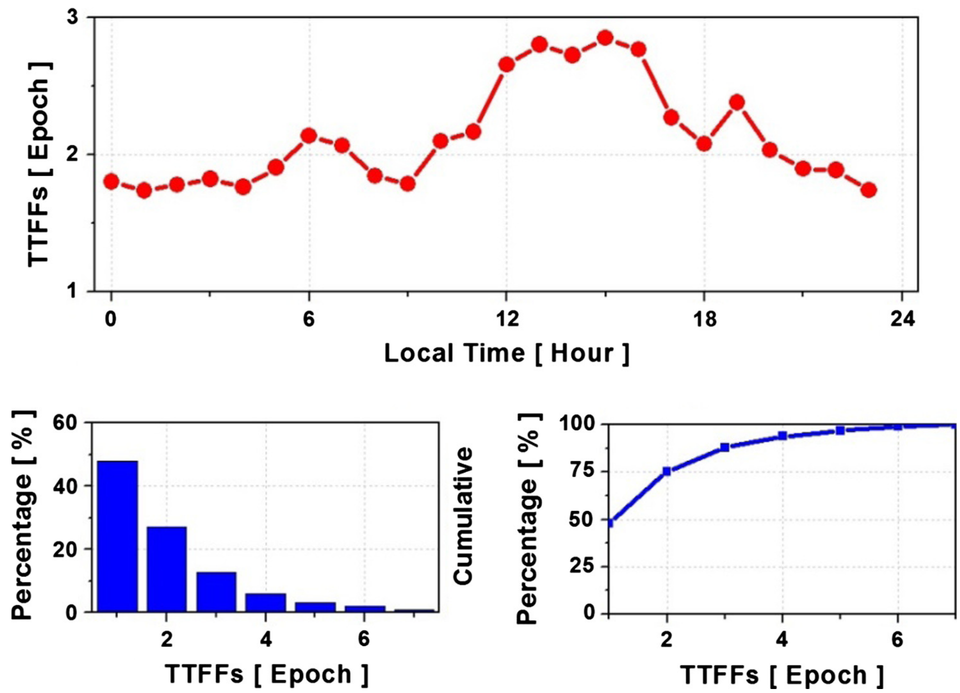

Fig. 3. Average TTFF of WL ambiguity for all baselines; Upper panel is the function of local time of hourly average values; Bottom panel is the corresponding histogram (left) and cumulative distribution function (right) of the average values.

(around local time 14:00). The average TTFF of WL ambiguity during high ionospheric activity is almost twice that of the TTFF of WL ambiguity during quieter times. This is mainly attributed to that DD ionospheric delays are set as zero initially and then estimated as random walk. Thus, an active ionospheric delay generally means a larger initial bias and variance than other time. Moreover, in approximately 50% of the epochs, WL ambiguities are successfully fixed by 1 epoch and in approximately 90% of the epochs, WL ambiguities are fixed within 4 epochs. All the WL ambiguities are fixed within 7 epochs.

Fig. 4 gives the average TTFF of NL AR of all baselines, which explains more about NL AR. In upper panel, it is clear that it takes more time to fix NL ambiguities around local time 14:00, which is the same to WL ambiguity. It only takes approximately 4 epochs to fix NL ambiguity when ionospheric activity is low. However, 7–12 epochs are needed to fix NL ambiguity when ionospheric activity is high. The bottom panel illustrates the distribution of average TTFF of NL. To make the results more clear, TTFF is counted as 40 when it is larger than 40. These results demonstrate that approximately 60% of NL ambiguities are fixed within 5 epochs and 90% of NL ambiguities are fixed within 30 epochs. All these are very promising results for TTFFs.

3.3. Rapid re-convergence

In situations with the loss of satellite lock, unstable communication links and poor environmental conditions, rover receivers may lose the observables from the base station, which forces the RTK system to re-converge on a position. If we have already fixed the ambiguities before, the atmospheric information obtained by NL fixed solution can help to speed up the re-convergence. Hence, we analyze the re-convergence with prior atmospheric information. Considering a short time that rover receivers lose connection from base station and vertical ionospheric delay is almost stable within 5 min in most situation (Shi et al., 2012), we analyze re-convergence time by using atmospheric delay derived from 5 min previous. In order to simulate this situation, we first compute the precise atmospheric delay information with station coordinate fixed and save it in a temporary file. Second, the kinematic positioning is processed epoch by epoch with the predicted atmospheric delay information by using data from 5 min previous. Like analysis of TTFFs, the Kalman filter is set to re-initialize when the NL-fixed solution is obtained in order to analyze the re-convergence time. The success rate is calculated by Eq. (9):

$$Fixed\ Percentage = \frac{n_{fixed}}{n_{total}} \times 100\% \tag{9}$$

where n_{total} is the number of total epochs of observables and n_{fixed} is the number of fixed epochs.

Fig. 5 is the results of re-convergence time by using 5-min forecast atmospheric delay information. Compared with the results shown in section *Time-to-first-fix*, great improvement occurs when using predicted atmospheric delay information. As Fig. 5 shows, approximately 86.04% of epochs can be fixed immediately and 90.27% of observables can be fixed within 2 epochs. Additionally, the performance differs slightly among different baselines. The best one is baseline B, which is located in the highest latitude (approximately 37°N) of these 8 baselines, with

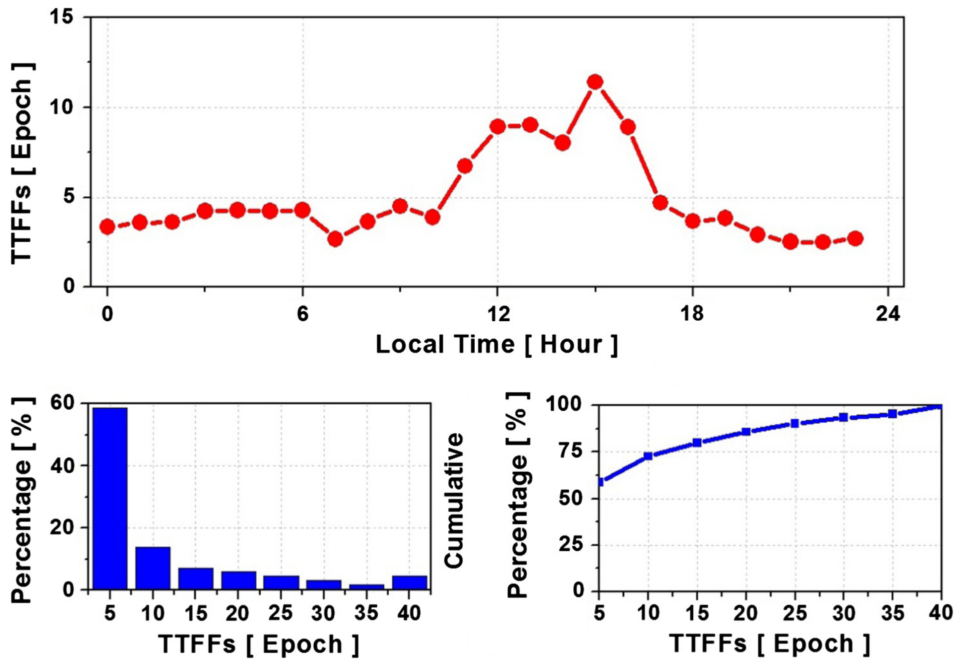

Fig. 4. Average TTFF of NL ambiguity for all baselines; the upper panel shows the hourly average TTFF values as a function of local time; the bottom panel shows the corresponding histogram (left) and cumulative distribution function (right) of the average values.

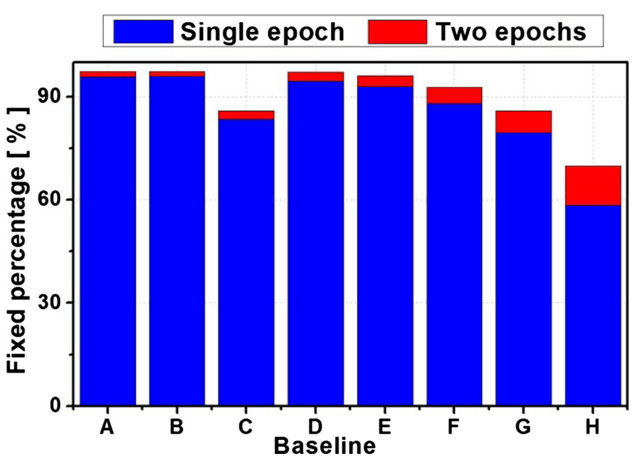

Fig. 5. Re-convergence analysis when the data gap is set as 5 min.

95.88% of epochs fixed by 1 epoch and 97.36% of epochs fixed within 2 epochs. This may be due to its mild atmospheric delay, which results in a more precise predicted atmospheric delay. On the other hand, baseline H, with a long distance (229 km) and low latitude (21° N) has the worst performance among these baselines: only 58.43% of epochs can be fixed instantaneously and 69.78% of epochs can be fixed within 2 epochs. Moreover, it should be noted that most unfixed epochs are concentrated in a high ionospheric activity time for all baselines, though it is not shown in the figure.

3.4. Positioning accuracy after TTFFs

Fig. 1 illustrates that we can obtain the EWL, WL and NL fixed solutions once their respective ambiguities are successfully fixed. It should also be noted that though the NL fixed solution can provide a more precise position, it requires a longer initial time than the EWL fixed solution (1 epoch) and the WL fixed solution (approximately 2 epochs). Thus, it is necessary to give a special focus on the EWL/WL/NL fixed solution.

Table 4 presents a summary of positioning accuracy statistics obtained in terms of East, North and Up components. For EWL fixed solution, the positioning differs much between different baselines. It is clear that positioning accuracy in low latitude area (e.g., baseline F, G and H) is worse than high latitude area and decreases with baseline distance. For example, the positioning accuracy of baseline E is 18.4, 15.5 and 26.4 cm for east, north and up component, respectively. However, the positioning accuracy decreases to 67.2, 157.2 and 102.1 cm for baseline G. Generally, the positioning accuracy is decimeter to meter level. For the WL fixed solution, the positioning accuracy is greatly improved, especially for baseline H and G. It seems that the average positioning accuracy is approximately 26 and 36 cm for horizontal and vertical components, respectively, and it only differs slightly among different baselines. As for the NL fixed solution, we can see that the positioning accuracy is in the same level for each baseline. The average positioning accuracies of the East, North and Up components of all baselines are approximately 1.6, 1.5 and 5.9 cm, respectively.

Fig. 6 gives an example of positioning errors of baseline B and F. It shows a clear improvement in positioning accuracy when NL ambiguities are fixed. Since we reset the filter once NL ambiguities are fixed, the tropospheric delay cannot be estimated well within a short time. Fig. 6 (red

Table 4
Summary of RMS statistics in terms of East, North and Up components of NL fixed solution of all baselines, (unit: cm).

Solution		A	B	C	D	E	F	H	G
EWL fixed	*East*	27.6	21.2	50.4	52.1	18.4	30.9	32.9	67.2
	North	38.2	26.2	45.9	44.1	15.5	**72.9**	**82.7**	**157.2**
	Up	53.3	41.0	74.7	61.4	26.4	40.8	48.5	**102.1**
WL fixed	*East*	18.8	14.5	21.3	22.3	13.6	17.7	19.0	24.4
	North	19.9	15.6	22.0	16.3	10.7	18.5	21.3	18.0
	Up	39.8	31.2	41.8	37.6	23.1	34.9	34.9	45.7
NL fixed	*East*	1.1	1.6	1.8	1.6	1.3	1.5	1.6	1.9
	North	1.5	1.2	1.5	1.5	1.4	1.7	1.6	1.7
	Up	3.9	9.6	6.1	6.2	3.7	5.1	5.3	6.9

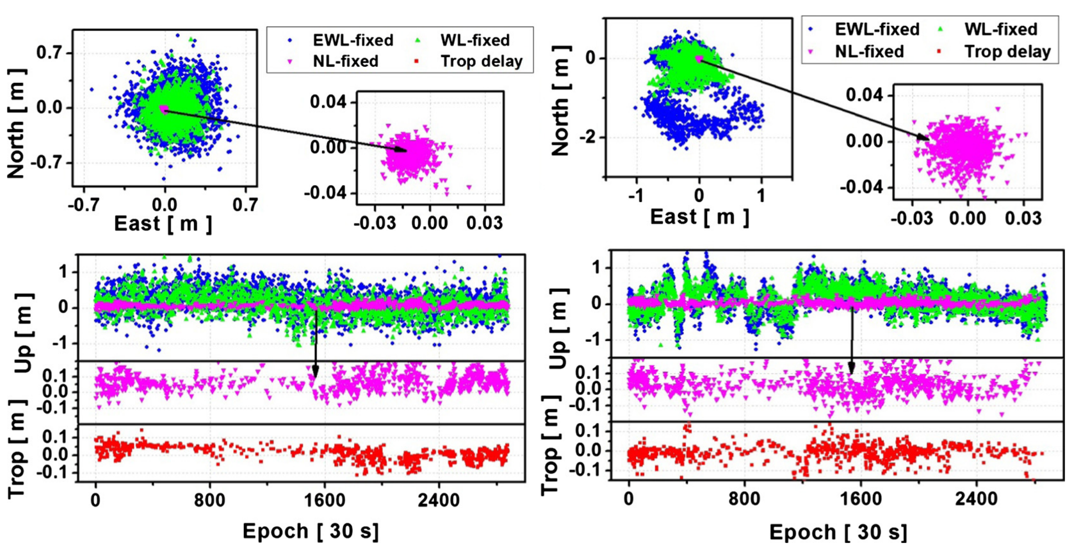

Fig. 6. Positioning results after TTFF; left panels are baseline B and right panels are baseline F; red points are tropospheric delay solution, blue, green and magenta points are the EWL, WL and NL fixed solution, respectively. (For interpretation of the references to color in this figure legend, the reader is referred to the web version of this article.)

points) illustrates clearly that the estimated tropospheric delay has a large noise component and biases of a few centimeters. Thus, the vertical component is obviously worse than the horizontal component.

4. Summary and conclusions

In this paper, we present a rapid AR performance based on GPS/BDS and dual/triple frequency observables for medium-long baseline RTK. Considering the large residual of DD atmospheric delay, a general model estimating atmospheric delay based on DD uncombined observables (i.e., L1/L2 and B1/B2/B3 observables) is employed. Because the model is based on DD uncombined observables, it can be extended well to additional satellite navigation systems (e.g., Galileo, QZSS). In order to resolve ambiguity rapidly and reliably, ambiguities are divided into three types (EWL, WL and NL) according to their wavelengths and are fixed step by step. Furthermore, a partial AR strategy is applied with a changing cut-off angle because the low-elevation observables are generally involved with large multipath and atmospheric delay residuals. Hence, ambiguities can be resolved to integers rapidly and reliably. Moreover, once NL fixed solution is obtained, we can estimate the precise atmospheric delay. This can help rapid re-convergence when the rover receiver loses connection with the base station for a short time (e.g., 5 min).

Several baselines collected by two types of receivers (Trimble Net R9 and Panda) with distances ranging from 61 to 232 km are used to test the proposed method. The experiment focuses on three aspects: TTFF, rapid re-convergence and positioning accuracy after TTFF.

(1) The results show the expected performance, that the average TTFFs of EWL, WL and NL ambiguities are 1, 2 and 6 epochs (interval: 30 s), respectively. Atmospheric activity is still the main factor that affects AR. More epochs are clearly necessary to fix WL and NL ambiguities around local time 14:00–15:00 than at other times.

(2) With respect to the re-convergence time, we simulate a scenario in which a rover receiver loses connection with base station for 5 min. The predicted atmospheric delay is shown to greatly benefit rapid re-convergence: 86% of observables can be fixed instantly and 90% of observables can be fixed within two epochs. This performance differs among different baselines mainly due to different ionospheric delay activities, which directly affect the precision of predicted ionospheric delay.
(3) Limited by the large atmospheric delay, the positioning accuracy is about decimeter to meter levels for the EWL fixed solution, but it is greatly improved when WL ambiguities are fixed. The average positioning accuracies are approximately 26 and 36 cm for the horizontal and vertical components, respectively. Once the NL ambiguities are fixed, we are able to obtain centimeter-level positioning accuracy. The statistical positioning accuracy of East, North and Up components are approximately 1.6, 1.5 and 5.9 cm, respectively.

Acknowledgments

This study is partially supported by the National Key Research and Development Plan (No. 2016YFB0501803), the National Natural Science Foundation of China (41374034, 41504028 and 41204030), the Natural Science Foundation of China (2014AA123101), the Natural Science Foundation of Hubei (2015CFB326) and the Fundamental Research Funds for the Central Universities (2042014kf0081). Also, thanks also due to S. Verhagen and B. Li for providing LAMBDA–Matlab, version 3.0. The authors greatly appreciate the constructive and useful comment from reviewers.

References

Bock, Y., Gourevitch, S.A., Counselman, C.C., King, R.W., Abbot, R.I., 1986. Interferometric analysis of GPS phase observations. Manuscripta Geod. 11 (4), 282–288.
Cannon, M.E., Lachapelle, G., Alves, P., Fortes, L.P., Townsend, B., 2001. GPS RTK Positioning using a regional reference network: theory and results. Proceedings of the 5th GNSS International Symposium, Seville, (CD-ROM) 8–11 May 2001.
Chu, F.Y., Yang, M., 2014. GPS/Galileo long baseline computation: method and performance analyses. GPS Solut. 18 (2), 263–272.
Dekkiche, H., Kahlouche, S., Abbas, H., 2010. Differential ionosphere modeling for single-reference long-baseline GPS kinematic positioning. Earth Planets Space 62 (12), 915–922.
Deng, C., Tang, W., Liu, J., Shi, C., 2014. Reliable single-epoch ambiguity resolution for short baselines using combined GPS/BeiDou system. GPS Solut. 18 (3), 375–386.
Euler, H., Goad, C., 1991. On optimal filtering of GPS dual frequency observations without using orbit information. Bull. Geod. 65 (2), 130–143.
Feng, Y., 2008. GNSS three carrier ambiguity resolution using ionosphere-reduced virtual signals. J. Geod. 82 (12), 847–862.
Feng, Y., Rizos, C., 2005. Three carrier approaches for future global regional and local GNSS positioning services: concepts and performance Perspectives. Proceedings of ION GNSS 2005, 13-16 September, Long Beach, CA, pp. 2277–2787.
Forssell, B., Martin-Neira, M., Harrisz, R.A., 1997. Carrier phase ambiguity resolution in GNSS-2. Proceedings of the ION GPS-97, 16-19 September, Kansas City, MO, pp. 1727–1736.
He, H., Li, J., Yang, Y., Xu, J., Guo, H., Wang, A., 2014. Performance assessment of single- and dual-frequency BeiDou/GPS single-epoch kinematic positioning. GPS Solut. 18 (3), 393–403.
Hu, G.R., Khoo, H.S., Goh, P.C., Law, C.L., 2003. Development and assessment of GPS virtual reference stations for RTK positioning. J. Geod. 77 (5), 292–302.
Jin, S.G., Wang, J., Park, P.H., 2005. An improvement of GPS height estimations: stochastic modeling. Earth Planets Space 57 (4), 253–259.
Jin, S.G., Luo, O.F., Ren, C., 2010. Effects of physical correlations on long-distance GPS positioning and zenith tropospheric delay estimates. Adv. Space Res. 46 (2), 190–195.
Jung, J., 1999. High integrity carrier phase navigation for future LAAS using multiple civilian GPS signals. Proc. ION GPS-1999, Institute of Navigation, Nashville, Tennessee, Alexandria, pp. 14–17.
Lou, Y., Gong, X., Gu, S., Zheng, F., Feng, Y., 2016. Assessment of code bias variations of BDS triple-frequency signals and their impacts on ambiguity resolution for long baselines. GPS Solut. http://dx.doi.org/10.1007/s10291-016-0514-4.
Odijk, D., 2000. Weighting ionospheric corrections to improve fast GPS positioning over medium distances. Proceedings of the ION GPS, 19–22 September, Salt Lake City, UT, pp. 1113–1123.
Odolinski, R., Teunissen, P., Odijk, D., 2014. First combined COMPASS/BeiDou-2 and GPS positioning results in Australia. Part II: Single- and multiple-frequency single-baseline RTK positioning. J. Spat. Sci. 59 (1), 25–46.
Paziewski, J., 2015. Study on desirable ionospheric corrections accuracy for network-RTK positioning and its impact on time-to-fix and probability of successful single-epoch ambiguity resolution. Adv. Space Res. 57 (4), 1098–1111.
Rao, C., 1973. Linear Statistical Influence and its Applications. Wiley, New York.
Rizos, C., 2002. Network RTK research and implementation: a geodetic perspective. J. GPS 2 (1), 144–150.
Shi, C., Gu, S., Lou, Y., Ge, M., 2012. An improved approach to model ionospheric delays for single-frequency precise point positioning. Adv. Space Res. 49 (12), 1698–1708.
Tang, W., Deng, C., Shi, C., Liu, J., 2015. Triple-frequency carrier ambiguity resolution for Beidou navigation satellite system. GPS Solut. 18 (3), 335–344.
Teunissen, P., 1995. The least-squares ambiguity decorrelation adjustment a method for fast GPS integer ambiguity estimation. J. Geod. 70 (1), 65–82.
Teunissen, P., 1997. The geometry-free GPS ambiguity search space with a weighted ionosphere. J Geod. 71 (6), 370–383.
Teunissen, P., Joosten, P., Tiberius, C., 2002. A comparison of TCAR, CIR and LAMBDA GNSS ambiguity resolution. Proceedings of the ION GPS, 24–27 September, Portland, OR, pp. 2799–2808.
Teunissen, P., Odolinski, R., Odijk, D., 2014. Instantaneous BeiDou +GPS RTK positioning with high cut-off elevation angles. J. Geod. 88 (4), 335–350.
Tiberius, C.C.J.M., Pany, T., Eissfeller, B., Joosten, P., Verhagen, S., 2002. 0.99999999 Confidence ambiguity resolution with GPS and Galileo. GPS Solut. 6 (1), 96–99.
Verhagen, S., 2002. Performance analysis of GPS, galileo and integrated GPS-galileo. Proceedings of ION GPS 2002, Portland, Oregon, September 24–27, pp. 2208–2215.
Verhagen, S., Teunissen, P., 2013. The ratio test for future GNSS ambiguity resolution. GPS Solut. 17 (4), 535–548.
Vollath, U., 2004. The factorized multi-carrier ambiguity resolution (FAMCAR) approach for efficient carrier-phase ambiguity estimation.

Proceedings of ION GNSS 2004, 21–24 September, Long Beach, CA, pp. 2499–2508.

Xu, Y., Ji, S., Chen, W., Weng, D., 2015. A new ionosphere-free ambiguity resolution method for long-range baseline with GNSS triple-frequency signals. Adv. Space Res. 56 (8), 1600–1612.

Yanase, T., Tanaka, H., Ohashi, M., Kubo, Y., Sugimoto, S., 2010. Long baseline relative positioning with estimating ionosphere and troposphere gradients. 23rd International Technical Meeting of the Satellite Division of The Institute of Navigation, Portland, OR, September 21–24, pp. 196–206.

Yang, M., Tang, C.H., Yu, T.T., 2000. Development and assessment of a medium-range real-time kinematic GPS algorithm using an ionospheric information filter. Earth Planet Space 52 (10), 783–788.